

# SUPPORTING INFORMATION

## Rationalization of the Membrane Permeability Differences in a Series of Analogue Cyclic Decapeptides

Jagna Witek,<sup>†</sup> Shuzhe Wang,<sup>†</sup> Benjamin Schroeder,<sup>†</sup> Robin Lingwood,<sup>†</sup> Andreas Dounas,<sup>†</sup> Hans-Jörg Roth,<sup>‡</sup> Marianne Fouché,<sup>‡</sup> Markus Blatter,<sup>‡</sup> Oliver Lemke,<sup>¶</sup> Bettina Keller,<sup>¶</sup> and Sereina Riniker<sup>\*,†</sup>

*<sup>†</sup>Laboratory of Physical Chemistry, ETH Zürich, Vladimir-Prelog-Weg 2, 8093 Zürich,  
Switzerland*

*<sup>‡</sup>Novartis Institutes for BioMedical Research, Novartis Pharma AG, Novartis Campus,  
4056 Basel, Switzerland*

*<sup>¶</sup>Department of Biology, Chemistry, Pharmacy, Freie Universität Berlin, Takustrasse 3,  
14195 Berlin, Germany*

E-mail: [sriniker@ethz.ch](mailto:sriniker@ethz.ch)

# Experimental Details

## NMR Measurements

### Sample Preparation

1-2 mg of lyophilized peptides were dissolved in 40  $\mu$ l de-acidified CDCl<sub>3</sub>, vortexed for 20 s and transferred into 1.7 mm Sample Jet NMR sample tubes. Samples were spun down into the tube using a Hettich manual centrifuge. Tubes were then closed by pressing a POM ball into the funnel of the tube cap. Tubes were then inserted into 1.7 mm shuttles and placed on the automatic sample changer.

### Data Acquisition and Processing

<sup>1</sup>H detected 1D and 2D NMR spectra were obtained using a Bruker 600 MHz AVANCE III spectrometer equipped with a 1.7 mm TCI cryo probe and a z-gradient system. 1D proton spectra were recorded with a standard one-pulse sequence (30 degree flip angle) with a relaxation delay of 1 s and an acquisition time of 2.73 s. 16 scans of 65536 points covering 12019.23 Hz were recorded. For determination of amide temperature coefficients data was recorded in a range of 290 to 320 K for DMSO and 275 to 310 K for chloroform, respectively. Data was zero-filled to 65536 complex points and an exponential window function was applied with a line-broadening factor of 0.3 Hz prior to Fourier transformation.

All 2D experiments for NMR assignment were recorded at a temperature of 300K with a relaxation delay of 1.5 s. For gradient COSY spectra<sup>1,2</sup> a data matrix of 512 x 2048 points covering 6602.1 x 6602.1 Hz was recorded with one scan for each increment. Data was linear predicted to 1024 x 2048 points using 32 coefficients and zero filled to 2048 x 2048 points. A sine square bell shaped window function was applied in F2 and a cosine square bell shaped window function in F1, respectively, prior to magnitude mode type 2D Fourier transformation. For edited coherence order selective gradient HSQC spectra<sup>3,4</sup> using adiabatic inversion pulses on the carbon channel,<sup>5</sup> a data matrix of 256 x 2048 points covering 24901 x 8417.5 Hz was recorded using two scans for each increment. Data was linear predicted to 512 x 2048 points using 32 coefficients and zero filled to 1024 x 2048 points prior to echo-anti echo type 2D Fourier transformation. A sine square bell shaped window function shifted by  $\pi/2$  in both dimensions was applied. For HMBC spectra,<sup>6</sup> a data matrix of 256 x 4096 points covering 33805 x 8417.5 Hz with 4 scans for each increment was recorded using a double low pass J-filter and F1 absorption mode.<sup>7</sup> Data was linear predicted to 512 x 4096 points using 32 coefficients and zero-filled to 1024 x 2048 complex points prior to echo-anti echo type 2D Fourier transformation. A cosine square shaped window function was applied in F1 and a sine shaped window function shifted by  $\pi/4$  was applied in F2. Data was converted to magnitude mode in F2 prior to analysis. ROESY spectra<sup>8,9</sup> with an effective field of  $\gamma$ B1 = 8333 Hz and an spin lock time of 200 ms were recorded for a data matrix of 512 x 2048 points covering 8417.5 x 8417.5 Hz. Four scans were recorded for each increment. Data was linear predicted to 1024 x 2048 points using 32 coefficients prior to States-TPPI type 2D Fourier transformation and a sine square bell shaped window function shifted by  $\pi/2$  in both dimensions was applied. For MLEV-17 based TOCSY spectra,<sup>10</sup> a data matrix of 256 x 2048 points covering 8417.5 x 8417.5 Hz with two scans were recorded for each increment. Data

was linear predicted to 512 x 2048 points using 32 coefficients and zero filled to 1024 x 2048 points prior to TPPI type 2D Fourier transformation. A cosine square bell shaped window function was applied in both dimensions. For determination of  $^nJ_{HC}$  couplings constants J-HMBC spectra<sup>11</sup> were acquired. A folded data matrix of 756 x 4096 points covering 15091.9 x 6602.1 Hz was recorded using 16 scans for each increment. A coupling evolution delay of 436.8 ms with a scaling factor of 17.5 was used. Data was linear predicted to 1512 x 4096 points using 32 coefficients and zero-filled to 2048 x 4096 complex points prior to echo-anti echo type 2D Fourier transformation. A cosine square shaped window function was applied in F1 and a sine shaped window function shifted by  $\pi/4$  was applied in F2. Data was converted to magnitude mode in F2 prior to analysis. For determination of coupling constants relevant 1D traces along F1 were extracted using Topspin 3.2 (Bruker Biospin). For T2 relaxation measurements, a pseudo 2D CPMG (Carr-Purcell-Meiboom-Gill) sequence<sup>12</sup> was used. 20 different echo times up to a maximum 1 s were recorded with a relaxation delay of 20 s using 16 scans of 6144 points covering 12019.23 Hz. Data was zero-filled to 8192 complex points and an exponential window function was applied with a line-broadening factor of 1.0 Hz prior to Fourier transformation. Relaxation times were determined by exponential line fitting using Dynamics Center software package (Version 2.3.3, Bruker Biospin). All spectra were referenced according to the internal solvent signal ( $^1H$ : CDCl<sub>3</sub> = 7.26 ppm and  $^{13}C$ : CDCl<sub>3</sub> = 77.16 ppm).<sup>13</sup>

## Resonance Assignment

1D and 2D spectra were imported into the NMR workbook of ACD Spectrus 2014 for resonance assignment. 1D, HSQC and TOCSY were analyzed to assign protons and carbons of individual amino acid spin systems. Sequential connectivity assignments were achieved using 2D-NOESY experiments.

## Structure Calculation

Initial peak picking and nOe assignments were performed using the ATNOSCANDID package.<sup>14,15</sup> Peak lists of the first cycle were used as an input for the program CYANA 3.97.<sup>16</sup> The “noeassign” protocol of CYANA was used to assign and calibrate the nOe signals of the given peak lists in presence of dihedral restraints based on homo and hetero  $^3J$  scalar couplings using the Karplus equation. These lists were cleaned by applying a cutoff for the quality factor of 0.6 and by reviewing the peak lists and inspection of the NOESY spectra. Further the restraints were mirrored according the molecular symmetry. The final NOE upper distance bounds are given in Tables S3 -S8.

The AMBER 14 package<sup>17</sup> was used for structure refinement using semi-quantum mechanically derived force field parameters by antechamber4 and implicit solvent (GB Neck variant of the generalized Born model<sup>18</sup>) using a dielectric constant of four reflecting the non-polar chloroform. Harmonic square-well penalty functions with force constants of 10 kcal mol<sup>-1</sup> Å<sup>-2</sup> for all distance constraints were applied. An exception was made for the distance restraints between the *N*-methyl groups (*i*) and alpha protons (*i*-1) of trans the peptide bonds. In these cases, the restraining force constant was set to 50 kcal mol<sup>-1</sup> Å<sup>-2</sup> to insure the correct conformation. First, a short minimization with long-range electrostatics treatment by

the particle mesh Ewald method<sup>19</sup> using steepest-descent energy minimization followed by conjugate-gradient minimization was performed. The minimized structures were then refined using a simulated annealing protocol of 30'000 steps. For all refinements, a 1 fs time step in combination with constraint bond lengths using SHAKE,<sup>20</sup> and a 15 Å nonbonded cutoff were used. Scaling factors for the 1-4 electrostatic and 1-4 nonbonded van der Waals interactions were set to default values (scee=1.2, scnb=2.0). For each peptide, all ten structures were refined in AMBER for the final ensembles. The first structure of each peptide, which was used as starting structure for the simulations, is given in the Supporting Information.

## PAMPA Permeability

The parallel artificial membrane permeation (PAMPA)<sup>21</sup> was used as a primary screen to predict the gastro-intestinal permeability. The assay was carried out in 96-well plates, measuring the ability of the compound to diffuse from a donor to an acceptor plate separated by a 9-10 μm hexadecane liquid layer coated on a polycarbonate filter plate. To minimize solubility issues, compounds were loaded at 5 μM in the donor compartment and the assay buffer contained 5% DMSO. The permeability was derived from the compound concentration measured by LC-MS/MS in the acceptor compartment after a 4-hour incubation time.

## LogD

The 1-octanol/water distribution coefficient at pH = 7.4 (logD) was determined using the Shake-Flask equilibrium method. Prior to start the experiment the two phases were pre-saturated, so “water-saturated octanol” and “octanol-saturated water” were used. The samples were first dissolved in 1-octanol at a target concentration of 1 mM. One vial was used for each phase concentration determination and the phase ratio  $K$  between the two phases was 10.0 (where  $K = V_{\text{water}}/V_{\text{octanol}}$ ). The duplicates vials were agitated on a rotator for 20 h at 75 rpm. Subsequently, vials were centrifuged for 15 min at 3600 rpm with positioning one vial with the caps at top and another vial turned upside down. The upside-down position allows the sampling of water by a syringe without the need to pass through the octanol phase and avoid any risk of contamination of the aqueous phase. An adequate dilution was made for the two phases (x2 for the aqueous phase, x2000 for the octanol phase) and the samples were quantified by LC-HRMS using a 6-points calibration curve (Vanquish coupled to an Exactive-Plus, Thermo Scientific). The column used was Zorbax\_SB\_AQ 30 x 2.1 mm 1.8 μm, and the column oven temperature was 40 °C.

## ADDITIONAL TABLES AND FIGURES

Table S1: The number of TICs used for the distance matrix calculation, the lagtimes  $\tau$  selected for construction of the CSMMs, and the parameters for the CNN clustering: nearest-neighbor distance (NND) and number of nearest neighbors (NNN). For an implementation of the CNN algorithm, see <https://github.com/BDGSoftware/CNNClustering>.

Peptide	H <sub>2</sub> O				CHCl <sub>3</sub>			
	TICs	$\tau$ [ns]	NND	NNN	TICs	$\tau$ [ns]	NND	NNN
MKI	5	5	0.20	3	4	5	0.10	10
MII	7	15	0.30	25	3	20	0.15	2
MHQ	5	6	0.30	15	5	3	0.15	2
MDP	5	20	0.15	5	3	30	0.25	10
MDR	2	4	0.05	15	13	4	0.20	10
MJI	5	3	0.20	5	5	4	0.25	3

Table S2: Root mean square fluctuations (RMSF) for all C <sub>$\alpha$</sub>  in the initial 100-ns simulations in water, chloroform and DMSO.

Amino acid nr.	MKI			MII			MHQ		
	CHCl <sub>3</sub>	DMSO	H <sub>2</sub> O	CHCl <sub>3</sub>	DMSO	H <sub>2</sub> O	CHCl <sub>3</sub>	DMSO	H <sub>2</sub> O
1	0.046	0.125	0.044	0.046	0.052	0.043	0.045	0.107	0.108
2	0.055	0.146	0.051	0.055	0.062	0.049	0.054	0.125	0.132
3	0.054	0.120	0.046	0.053	0.066	0.044	0.054	0.086	0.093
4	0.052	0.063	0.048	0.054	0.057	0.048	0.054	0.058	0.053
5	0.061	0.102	0.057	0.062	0.065	0.055	0.062	0.064	0.073
6	0.043	0.123	0.044	0.043	0.058	0.042	0.046	0.080	0.061
7	0.052	0.138	0.051	0.054	0.063	0.049	0.056	0.116	0.109
8	0.056	0.120	0.046	0.054	0.065	0.044	0.055	0.084	0.100
9	0.055	0.060	0.048	0.055	0.058	0.048	0.054	0.063	0.052
10	0.063	0.092	0.055	0.062	0.065	0.055	0.062	0.067	0.083
Amino acid nr.	MDP			MDR			MJI		
	CHCl <sub>3</sub>	DMSO	H <sub>2</sub> O	CHCl <sub>3</sub>	DMSO	H <sub>2</sub> O	CHCl <sub>3</sub>	DMSO	H <sub>2</sub> O
1	0.044	0.129	0.106	0.042	0.101	0.138	0.043	0.086	0.088
2	0.054	0.125	0.151	0.050	0.086	0.134	0.052	0.079	0.106
3	0.053	0.121	0.144	0.051	0.078	0.154	0.056	0.096	0.146
4	0.053	0.060	0.055	0.053	0.050	0.063	0.055	0.043	0.047
5	0.060	0.095	0.101	0.059	0.068	0.107	0.063	0.076	0.110
6	0.044	0.138	0.129	0.045	0.089	0.137	0.046	0.087	0.087
7	0.053	0.148	0.159	0.054	0.078	0.136	0.055	0.083	0.106
8	0.052	0.143	0.138	0.052	0.077	0.147	0.057	0.092	0.144
9	0.053	0.085	0.060	0.051	0.052	0.060	0.052	0.044	0.047
10	0.059	0.131	0.099	0.060	0.074	0.101	0.064	0.076	0.108

Table S3: NOE upper distance bounds of peptide **1** in chloroform.

Index	Residue 1	Residue 2	Upper bound [nm]	Index	Residue 1	Residue 2	Upper bound [nm]	Index	Residue 1	Residue 2	Upper bound [nm]
1	2 HA	6 HN	0.537	31	1 HN	2 HB@	0.491	61	10 HB	9 HG1	0.600
2	3 HN	6 HA	0.476	32	1 HN	1 HG	0.335	62	9 HG1	9 HD1	0.271
3	1 HN	8 HA	0.537	33	1 HN	1 HD2@	0.434	63	9 HG1	9 HD2	0.344
4	3 HA	6 HN	0.491	34	1 HN	1 HD1@	0.494	64	9 HG1	8 HD1@	0.513
5	1 HN	8 HD1@	0.574	35	10 HA	9 HG@	0.578	65	3 HD2@	4 HG1	0.519
6	1 HN	8 HD2@	0.600	36	1 HN	1 HB@	0.312	66	4 HG1	5 HE@	0.600
7	1 HN	8 HG	0.399	37	1 HB@	10 HCN@	0.376	67	4 HG1	5 HD@	0.578
8	3 HB@	6 HN	0.443	38	3 HN	3 HB@	0.301	68	4 HG1	4 HA	0.433
9	3 HN	6 HB2	0.435	39	3 HG	4 HA	0.524	69	4 HD1	4 HG1	0.266
10	1 HN	9 HA	0.379	40	10 HG2@	1 HN	0.498	70	9 HB1	8 HD1@	0.563
11	7 HCN@	5 HA	0.468	41	5 HA	5 HE@	0.506	71	9 HA	9 HB1	0.240
12	3 HN	5 HA	0.596	42	5 HA	5 HB2	0.305	72	9 HB1	9 HD2	0.362
13	1 HG	9 HA	0.548	43	4 HB1	5 HA	0.427	73	10 HCN@	9 HB1	0.432
14	10 HCN@	8 HG	0.472	44	10 HG2@	1 HA	0.504	74	9 HA	9 HB2	0.302
15	1 HN	9 HD1	0.586	45	6 HA	6 HB2	0.304	75	10 HCN@	9 HB2	0.412
16	4 HD1	6 HN	0.546	46	3 HA	4 HD2	0.226	76	10 HA	9 HB2	0.492
17	2 HA	4 HD1	0.554	47	9 HD1	8 HB2	0.401	77	9 HB2	9 HD1	0.406
18	2 HA	4 HD2	0.548	48	9 HD1	8 HN	0.484	78	9 HB2	9 HD2	0.420
19	4 HD2	6 HN	0.566	49	10 HA	9 HD1	0.595	79	9 HA	9 HG2	0.343
20	1 HN	9 HG1	0.584	50	9 HD1	8 HD1@	0.562	80	9 HG2	9 HD1	0.369
21	1 HN	9 HB2	0.583	51	9 HD1	8 HD2@	0.600	81	9 HG2	9 HD2	0.279
22	1 HD2@	9 HB2	0.600	52	3 HN	4 HD1	0.450	82	4 HB2	5 HA	0.575
23	10 HCN@	8 HB1	0.528	53	4 HD1	5 HA	0.543	83	4 HD1	4 HB2	0.360
24	1 HN	2 HA	0.468	54	4 HD1	4 HB1	0.338	84	5 HCN@	4 HB2	0.466
25	10 HA	1 HN	0.295	55	3 HG	4 HD2	0.429	85	8 HA	8 HB1	0.291
26	1 HN	10 HCN@	0.263	56	5 HB1	5 HE@	0.507	86	9 HD2	8 HB1	0.462
27	5 HCN@	6 HN	0.294	57	5 HB1	5 HD@	0.285	87	6 HD@@	6 HN	0.419
28	6 HN	5 HA	0.279	58	6 HG	5 HB1	0.572	88	6 HD@@	5 HB1	0.465
29	4 HA	5 HA	0.425	59	6 HN	5 HB1	0.475	89	6 HD@@	5 HB2	0.562
30	5 HCN@	5 HA	0.318	60	6 HA	5 HB1	0.516				

Table S4: NOE upper distance bounds of peptide **2** in chloroform.

Index	Residue 1	Residue 2	Upper bound [nm]
1	6 HG	3 HA	0.463
2	8 HD1@	2 HCN@	0.456
3	6 HG	3 HN	0.428
4	6 HN	3 HB1	0.475
5	8 HD1@	1 HB2	0.425
6	8 HD1@	1 HB1	0.446
7	6 HD1@	3 HB1	0.437
8	6 HD2@	4 HD1	0.577
9	8 HB1	10 HCN@	0.547
10	5 HCN@	3 HB1	0.550
11	1 HA	2 HCN@	0.465
12	7 HCN@	6 HA	0.487
13	9 HA	10 HCN@	0.380
14	5 HCN@	4 HA	0.411
15	8 HD1@	7 HCN@	0.480
16	7 HB@	7 HCN@	0.321
17	10 HCN@	10 HB@	0.344
18	5 HB@	5 HCN@	0.375
19	7 HCN@	6 HB@	0.405
20	8 HA	9 HD1	0.426
21	4 HD2	3 HA	0.451
22	8 HA	9 HD2	0.426
23	4 HD1	3 HA	0.489
24	3 HN	3 HB1	0.406
25	6 HD2@	5 HB@	0.517
26	5 HA	4 HB2	0.506
27	4 HG@	4 HD2	0.471

 Table S5: NOE upper distance bounds of peptide **3** in chloroform.

Index	Residue 1	Residue 2	Upper bound [nm]	Index	Residue 1	Residue 2	Upper bound [nm]	Index	Residue 1	Residue 2	Upper bound [nm]
1	6 HN	3 HN	0.474	29	10 HCN@	1 HN	0.392	57	10 HG2@	9 HA	0.543
2	8 HN	1 HN	0.497	30	10 HCN@	9 HA	0.334	58	8 HA	9 HD1	0.350
3	8 HN	2 HA	0.354	31	5 HCN@	4 HA	0.360	59	5 HG2@	5 HCN@	0.398
4	8 HN	2 HB@	0.464	32	5 HA	5 HCN@	0.415	60	10 HG2@	10 HCN@	0.430
5	8 HB1	1 HB2	0.410	33	10 HCN@	10 HA	0.436	61	9 HG2	9 HB1	0.396
6	6 HG	3 HB1	0.494	34	7 HCN@	7 HA	0.408	62	9 HG2	9 HB2	0.396
7	8 HB1	1 HB1	0.559	35	7 HB@	8 HN	0.405	63	7 HB@	8 HG	0.483
8	8 HD1@	1 HB2	0.509	36	8 HN	8 HG	0.516	64	3 HG	2 HB@	0.516
9	6 HN	4 HA	0.530	37	3 HG	3 HN	0.547	65	2 HB@	1 HB2	0.527
10	9 HA	1 HN	0.600	38	6 HN	7 HB@	0.529	66	2 HB@	1 HD2@	0.485
11	5 HA	7 HB@	0.573	39	2 HB@	1 HN	0.588	67	8 HB1	8 HD1@	0.385
12	6 HN	4 HG1	0.563	40	6 HN	6 HG	0.408	68	3 HD1@	3 HB1	0.418
13	9 HG1	1 HN	0.599	41	7 HB@	8 HA	0.440	69	3 HD2@	2 HB@	0.432
14	6 HG	4 HG1	0.589	42	3 HA	2 HB@	0.466	70	1 HB1	1 HD2@	0.331
15	7 HB@	9 HG1	0.587	43	1 HA	1 HD2@	0.348	71	1 HD1@	1 HB2	0.362
16	5 HG2@	7 HB@	0.550	44	5 HB	5 HCN@	0.411	72	9 HD2	9 HB1	0.460
17	6 HD1@	8 HG	0.600	45	6 HG	5 HCN@	0.384	73	4 HG1	4 HD1	0.389
18	3 HG	1 HD1@	0.600	46	7 HCN@	7 HB@	0.344	74	4 HG1	4 HD2	0.389
19	3 HD1@	1 HB2	0.544	47	2 HB@	2 HCN@	0.368	75	5 HG1	6 HD2@	0.586
20	7 HB@	9 HD1	0.451	48	2 HCN@	1 HD2@	0.416	76	6 HB@	6 HD1@	0.341
21	6 HB@	8 HG	0.471	49	2 HCN@	1 HD1@	0.342	77	9 HD2	9 HB@	0.382
22	6 HA	7 HCN@	0.335	50	6 HD1@	7 HCN@	0.538	78	9 HG1	9 HB@	0.410
23	2 HCN@	1 HA	0.358	51	6 HB@	7 HCN@	0.361	79	9 HG2	9 HB@	0.345
24	8 HA	9 HA	0.534	52	4 HD@	3 HA	0.332	80	4 HB@	4 HD@	0.473
25	4 HA	3 HA	0.585	53	8 HN	8 HB1	0.420	81	4 HG2	4 HD@	0.418
26	9 HA	10 HA	0.600	54	1 HB2	1 HN	0.376	82	4 HG1	4 HD@	0.339
27	5 HA	4 HA	0.600	55	5 HG2@	5 HA	0.397	83	4 HD@	3 HD2@	0.451
28	3 HN	2 HA	0.353	56	10 HG2@	10 HA	0.426				

Table S6: NOE upper distance bounds of peptide **4** in chloroform.

Index	Residue 1	Residue 2	Upper bound [nm]	Index	Residue 1	Residue 2	Upper bound [nm]	Index	Residue 1	Residue 2	Upper bound [nm]
1	8 HN	1 HN	0.413	28	3 HB@	3 HN	0.416	55	6 HN	6 HB1	0.422
2	6 HN	3 HN	0.437	29	1 HB@	1 HN	0.401	56	8 HN	8 HB2	0.403
3	6 HN	2 HB@	0.505	30	7 HB@	8 HN	0.372	57	4 HD1	3 HA	0.301
4	8 HD1@	1 HN	0.439	31	3 HN	2 HB@	0.385	58	8 HA	9 HD2	0.292
5	6 HB1	3 HN	0.431	32	6 HN	7 HB@	0.472	59	10 HCN@	10 HB1	0.536
6	6 HB2	3 HN	0.463	33	6 HA	6 HG	0.414	60	5 HB1	5 HCN@	0.550
7	8 HB2	1 HN	0.459	34	6 HA	7 HB@	0.532	61	6 HB2	7 HA	0.449
8	6 HD1@	3 HG	0.374	35	2 HB@	1 HA	0.550	62	5 HA	4 HB2	0.485
9	6 HN	4 HA	0.449	36	1 HA	1 HD1@	0.499	63	4 HG2	4 HD1	0.326
10	6 HG	4 HA	0.550	37	8 HN	8 HG	0.421	64	9 HD1	9 HB1	0.413
11	5 HCN@	3 HG	0.482	38	6 HN	6 HG	0.399	65	4 HG1	4 HD1	0.387
12	4 HD1	2 HB@	0.383	39	1 HG	1 HN	0.449	66	9 HD1	9 HB2	0.388
13	4 HG2	2 HB@	0.467	40	3 HA	3 HG	0.370	67	8 HB2	9 HD2	0.461
14	6 HN	7 HCN@	0.547	41	6 HG	7 HCN@	0.492	68	4 HB2	4 HD2	0.509
15	2 HCN@	1 HN	0.550	42	2 HCN@	1 HG	0.519	69	10 HCN@	9 HB1	0.487
16	7 HA	8 HN	0.283	43	6 HG	5 HCN@	0.350	70	5 HCN@	4 HB1	0.525
17	3 HN	2 HA	0.317	44	10 HD@	10 HA	0.376	71	10 HCN@	9 HB2	0.465
18	6 HN	7 HA	0.550	45	2 HCN@	1 HB@	0.335	72	1 HD2@	1 HB@	0.305
19	2 HA	1 HN	0.550	46	6 HB@	5 HCN@	0.459	73	4 HG1	3 HD2@	0.480
20	6 HA	5 HCN@	0.523	47	2 HB@	2 HCN@	0.281	74	10 HD@	10 HB2	0.370
21	10 HCN@	9 HA	0.285	48	2 HCN@	1 HD1@	0.344	75	10 HD@	1 HD1@	0.497
22	5 HCN@	4 HA	0.308	49	6 HD2@	7 HCN@	0.452	76	5 HB2	5 HCN@	0.331
23	6 HN	5 HCN@	0.333	50	6 HD2@	5 HCN@	0.519	77	10 HCN@	10 HB2	0.347
24	10 HCN@	10 HA	0.400	51	4 HD1	3 HN	0.439	78	6 HB2	7 HCN@	0.319
25	7 HCN@	7 HA	0.413	52	8 HN	9 HD2	0.550	79	6 HD2@	6 HB2	0.366
26	6 HA	7 HCN@	0.284	53	4 HD2	3 HN	0.550	80	1 HD2@	1 HB@	0.385
27	2 HCN@	1 HA	0.309	54	1 HN	10 HB2	0.545				

Table S7: NOE upper distance bounds of peptide **5** in chloroform.

Index	Residue 1	Residue 2	Upper bound [nm]	Index	Residue 1	Residue 2	Upper bound [nm]	Index	Residue 1	Residue 2	Upper bound [nm]
1	8 HN	1 HN	0.368	65	5 HA	6 HN	0.360	129	7 HB@	8 HN	0.380
2	6 HN	3 HN	0.412	66	6 HN	7 HCN@	0.481	130	1 HG	1 HN	0.316
3	1 HN	7 HA	0.550	67	2 HCN@	1 HN	0.519	131	7 HA	8 HG	0.458
4	3 HN	6 HN	0.368	68	2 HA	1 HN	0.550	132	5 HA	6 HD1@	0.550
5	1 HN	8 HN	0.412	69	7 HCN@	7 HA	0.333	133	1 HD1@	10 HA	0.550
6	6 HN	2 HA	0.550	70	6 HA	7 HCN@	0.224	134	5 HA	6 HD2@	0.550
7	1 HN	7 HB@	0.550	71	2 HCN@	1 HA	0.242	135	1 HD2@	10 HA	0.550
8	8 HN	1 HB@	0.535	72	3 HA	4 HCN@	0.269	136	3 HG	4 HCN@	0.467
9	8 HN	1 HD@@	0.541	73	9 HCN@	8 HA	0.292	137	8 HN	8 HG	0.362
10	8 HB@	1 HN	0.448	74	4 HA2	5 HA	0.474	138	3 HA	3 HG	0.324
11	8 HD@@	1 HN	0.544	75	3 HA	4 HA2	0.528	139	8 HA	8 HG	0.374
12	6 HD@@	3 HN	0.544	76	10 HA	9 HA@	0.511	140	7 HCN@	8 HG	0.550
13	6 HN	3 HB@	0.535	77	9 HA@	8 HA	0.535	141	3 HG	2 HCN@	0.550
14	6 HN	2 HB@	0.550	78	9 HA@	8 HN	0.535	142	3 HN	3 HB@	0.330
15	3 HN	6 HB@	0.535	79	8 HN	7 HB@	0.356	143	3 HN	3 HD@@	0.451
16	3 HN	6 HD@@	0.541	80	8 HN	8 HD1@	0.516	144	3 HB@	4 HCN@	0.535
17	3 HB@	6 HN	0.448	81	3 HN	3 HD1@	0.497	145	3 HB@	4 HA1	0.535
18	3 HD@	6 HN	0.544	82	3 HN	3 HD2@	0.497	146	3 HD@@	4 HA1	0.544
19	1 HD@@	8 HN	0.544	83	8 HN	8 HD2@	0.516	147	3 HD@@	4 HA2	0.544
20	1 HN	8 HB@	0.535	84	8 HN	8 HG	0.518	148	4 HA1	5 HB@	0.534
21	6 HB1	3 HN	0.526	85	2 HB@	3 HN	0.380	149	5 HG@	5 HA	0.381
22	8 HB1	1 HN	0.514	86	6 HG	6 HN	0.316	150	5 HG@	6 HN	0.518
23	8 HB2	1 HN	0.514	87	2 HA	3 HG	0.458	151	5 HB@	5 HA	0.262
24	6 HB2	3 HN	0.550	88	10 HA	1 HD1@	0.550	152	5 HA	6 HD@@	0.479
25	1 HB1	8 HN	0.526	89	6 HD1@	5 HA	0.550	153	6 HN	6 HD@@	0.467
26	3 HB1	6 HN	0.514	90	10 HA	1 HD2@	0.550	154	6 HA	6 HB@	0.267
27	3 HB2	6 HN	0.514	91	6 HD2@	5 HA	0.550	155	6 HA	6 HD@@	0.252
28	1 HB2	8 HN	0.550	92	8 HG	9 HCN@	0.467	156	6 HB@	7 HCN@	0.298
29	9 HCN@	1 HN	0.484	93	3 HN	3 HG	0.362	157	6 HB@	7 HA	0.468
30	6 HN	4 HCN@	0.531	94	8 HA	8 HG	0.324	158	6 HD@@	7 HA	0.544
31	2 HA	4 HCN@	0.550	95	3 HA	3 HG	0.374	159	7 HA	8 HD@@	0.434
32	9 HA2	1 HN	0.524	96	2 HCN@	3 HG	0.550	160	2 HA	1 HD@@	0.544
33	6 HN	4 HA@	0.384	97	8 HG	7 HCN@	0.550	161	1 HN	10 HD@	0.377
34	4 HCN@	6 HN	0.484	98	8 HN	8 HB@	0.330	162	10 HA	10 HD@	0.428
35	1 HN	9 HCN@	0.531	99	8 HN	8 HD@@	0.451	163	9 HA@	8 HB@	0.519
36	7 HA	9 HCN@	0.550	100	8 HB@	9 HCN@	0.535	164	9 HA@	8 HD@@	0.485
37	4 HA2	6 HN	0.524	101	8 HB@	9 HA1	0.535	165	9 HCN@	8 HB@	0.535
38	1 HN	9 HA@	0.384	102	8 HD@@	9 HA1	0.544	166	8 HN	8 HB@	0.358
39	6 HG	4 HA@	0.533	103	8 HD@@	9 HA2	0.544	167	6 HN	5 HG1	0.550
40	1 HG	9 HA@	0.533	104	9 HA1	10 HB@	0.534	168	1 HB2	2 HA	0.550
41	8 HD@@	10 HD2	0.541	105	10 HG@	10 HA	0.381	169	7 HA	6 HB2	0.550
42	8 HD@@	10 HB@	0.456	106	10 HG@	1 HN	0.518	170	10 HD2	10 HA	0.409
43	3 HD@@	5 HD2	0.541	107	10 HB@	10 HA	0.262	171	6 HN	5 HB1	0.448
44	3 HD@@	5 HB@	0.456	108	10 HA	1 HD@@	0.479	172	6 HB1	6 HN	0.278
45	8 HN	9 HCN@	0.479	109	1 HN	1 HD@@	0.467	173	1 HB1	2 HA	0.550
46	4 HCN@	3 HN	0.518	110	1 HA	1 HB@	0.267	174	7 HA	6 HB1	0.550
47	2 HCN@	3 HN	0.492	111	1 HA	1 HD@@	0.252	175	6 HB1	5 HD@	0.510
48	10 HA	1 HN	0.360	112	1 HB@	2 HCN@	0.298	176	6 HG	5 HD@	0.389
49	1 HN	2 HCN@	0.481	113	1 HB@	2 HA	0.468	177	6 HD@@	5 HD@	0.478
50	7 HCN@	6 HN	0.519	114	1 HD@@	2 HA	0.544	178	5 HB1	4 HA@	0.535
51	7 HA	6 HN	0.550	115	2 HA	3 HD@@	0.434	179	5 HG2	5 HD@	0.259
52	2 HCN@	2 HA	0.333	116	7 HA	6 HD@@	0.544	180	1 HN	10 HG1	0.550
53	1 HA	2 HCN@	0.224	117	6 HN	5 HD@	0.377	181	6 HB2	7 HA	0.550
54	7 HCN@	6 HA	0.242	118	5 HA	5 HD@	0.428	182	2 HA	1 HB2	0.550
55	8 HA	9 HCN@	0.269	119	4 HA@	3 HB@	0.519	183	5 HD2	5 HA	0.409
56	4 HCN@	3 HA	0.292	120	4 HA@	3 HD@@	0.485	184	1 HN	10 HB1	0.448
57	9 HA2	10 HA	0.474	121	4 HCN@	3 HB@	0.535	185	1 HB1	1 HN	0.278
58	8 HA	9 HA2	0.528	122	3 HN	3 HB@	0.358	186	6 HB1	7 HA	0.550
59	5 HA	4 HA@	0.511	123	3 HN	2 HB@	0.356	187	2 HA	1 HB1	0.550
60	4 HA@	3 HA	0.535	124	3 HN	3 HD2@	0.516	188	1 HB1	10 HD@	0.510
61	4 HA@	3 HN	0.535	125	8 HN	8 HD2@	0.497	189	1 HG	10 HD@	0.389
62	3 HN	4 HCN@	0.479	126	8 HN	8 HD1@	0.497	190	1 HD@@	10 HD@	0.478
63	9 HCN@	8 HN	0.518	127	3 HN	3 HD1@	0.516	191	10 HB1	9 HA@	0.535
64	7 HCN@	8 HN	0.492	128	3 HN	3 HG	0.518	192	10 HG2	10 HD@	0.259

Table S8: NOE upper distance bounds of peptide **6** in chloroform.

Index	Residue 1	Residue 2	Upper bound [nm]	Index	Residue 1	Residue 2	Upper bound [nm]	Index	Residue 1	Residue 2	Upper bound [nm]
1	1 HN	8 HN	0.374	34	8 HA	7 HCN@	0.497	67	3 HN	3 HD1@	0.440
2	1 HN	7 HA	0.550	35	3 HA	4 HCN@	0.248	68	8 HD1@	8 HN	0.463
3	1 HB1	8 HN	0.439	36	9 HCN@	8 HA	0.286	69	1 HD1@	2 HCN@	0.438
4	3 HN	7 HB@	0.366	37	4 HCN@	4 HA	0.411	70	2 HCN@	3 HD1@	0.433
5	1 HN	8 HB1	0.525	38	5 HCN@	4 HA	0.248	71	5 HCN@	6 HD1@	0.482
6	1 HB1	8 HD1@	0.348	39	10 HCN@	9 HA	0.285	72	1 HD1@	10 HCN@	0.510
7	3 HB1	6 HD1@	0.364	40	3 HN	3 HB1	0.440	73	10 HB@	10 HCN@	0.275
8	1 HB2	8 HD1@	0.491	41	8 HB1	8 HN	0.438	74	1 HG	2 HCN@	0.369
9	3 HG	6 HD1@	0.399	42	5 HD@	6 HN	0.550	75	2 HCN@	2 HB@	0.282
10	3 HB2	6 HD1@	0.511	43	10 HD@	1 HN	0.550	76	7 HB@	7 HCN@	0.297
11	3 HD1@	6 HD1@	0.369	44	1 HN	1 HB1	0.504	77	4 HCN@	4 HB@	0.267
12	4 HA	6 HN	0.428	45	6 HG	6 HN	0.346	78	9 HB@	9 HCN@	0.296
13	10 HA	2 HB@	0.533	46	1 HN	2 HB@	0.475	79	10 HCN@	9 HB@	0.321
14	7 HB@	5 HA	0.550	47	7 HB@	6 HN	0.544	80	1 HD2@	2 HCN@	0.418
15	2 HB@	4 HCN@	0.431	48	6 HD2@	6 HN	0.434	81	9 HCN@	8 HD2@	0.538
16	1 HB2	3 HD1@	0.471	49	10 HB1	10 HA	0.278	82	10 HB@	9 HB@	0.550
17	10 HA	1 HN	0.346	50	5 HA	5 HB2	0.300	83	6 HD2@	5 HB1	0.550
18	1 HN	2 HA	0.515	51	1 HA	1 HG	0.336	84	1 HD2@	1 HB2	0.298
19	2 HA	3 HN	0.270	52	3 HA	3 HB2	0.290	85	6 HD2@	6 HB1	0.322
20	8 HN	7 HA	0.286	53	2 HA	3 HD1@	0.528	86	1 HB1	1 HD1@	0.325
21	1 HA	2 HA	0.503	54	8 HD1@	7 HA	0.550	87	6 HB2	6 HD1@	0.341
22	7 HA	6 HA	0.539	55	9 HA	8 HD2@	0.550	88	10 HD@	10 HB1	0.361
23	10 HA	1 HA	0.468	56	3 HN	3 HG	0.426	89	5 HD@	5 HB1	0.322
24	6 HA	5 HA	0.506	57	8 HG	8 HN	0.452	90	10 HD@	10 HB2	0.298
25	5 HCN@	5 HA	0.392	58	3 HA	3 HG	0.360	91	5 HD@	6 HD2@	0.370
26	5 HCN@	6 HA	0.550	59	8 HA	8 HG	0.384	92	1 HD2@	1 HB1	0.402
27	1 HA	10 HCN@	0.550	60	1 HB2	2 HCN@	0.340	93	3 HB1	3 HD1@	0.289
28	3 HN	4 HCN@	0.367	61	3 HG	4 HCN@	0.492	94	1 HB2	1 HD1@	0.342
29	5 HCN@	6 HN	0.307	62	9 HCN@	8 HG	0.539	95	6 HB1	6 HD1@	0.374
30	2 HCN@	2 HA	0.404	63	5 HCN@	6 HG	0.476	96	3 HD2@	3 HB2	0.293
31	1 HA	2 HCN@	0.257	64	10 HD@	10 HA	0.380	97	8 HB1	8 HD1@	0.317
32	7 HCN@	6 HA	0.280	65	5 HD@	5 HCN@	0.317				
33	2 HCN@	3 HA	0.472	66	5 HE@	5 HCN@	0.317				

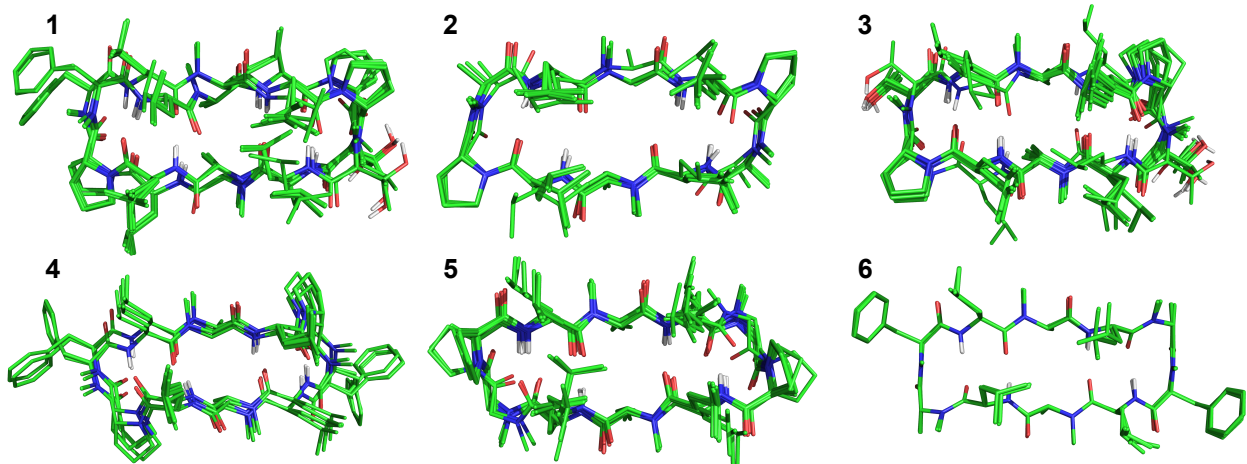


Figure S1: NMR bundles of the decapeptides in chloroform. (A) MKI, (B) MII, (C) MHQ, (D) MDP, (E) MDR, (F) MJI.

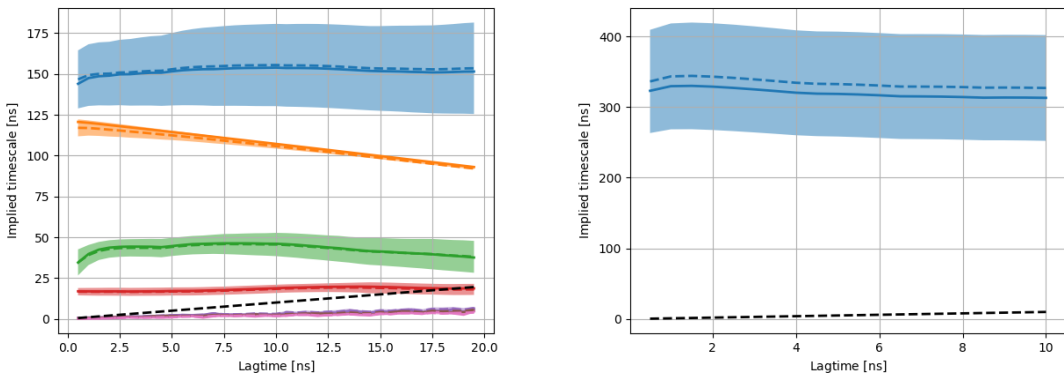


Figure S2: Implied time scales (ITS) for the interconversion processes of peptide **1** as described by CSMMs in water (left) and chloroform (right). The ITS of the whole data set is shown as solid line. The average (dashed line) and standard deviation (shaded area) were estimated with bootstrapping.

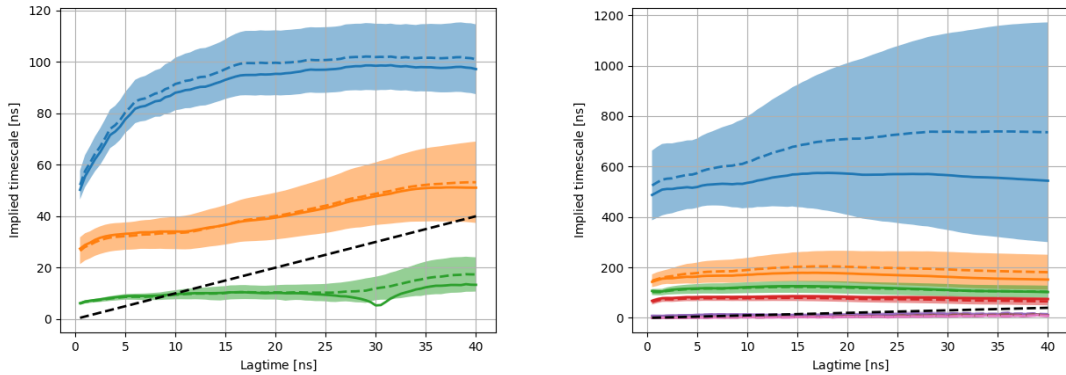


Figure S3: Implied time scales (ITS) for the interconversion processes of peptide **2** as described by CSMMs in water (left) and chloroform (right). The ITS of the whole data set is shown as solid line. The average (dashed line) and standard deviation (shaded area) were estimated with bootstrapping.

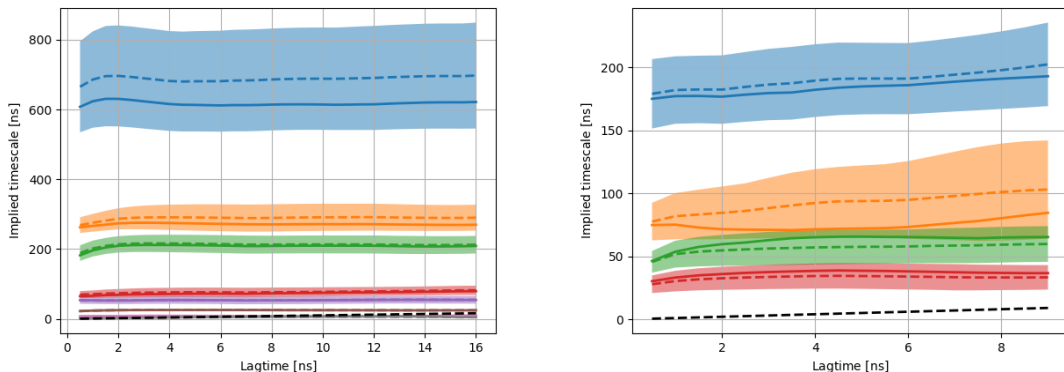


Figure S4: Implied time scales (ITS) for the interconversion processes of peptide **3** as described by CSMMs in water (left) and chloroform (right). The ITS of the whole data set is shown as solid line. The average (dashed line) and standard deviation (shaded area) were estimated with bootstrapping.

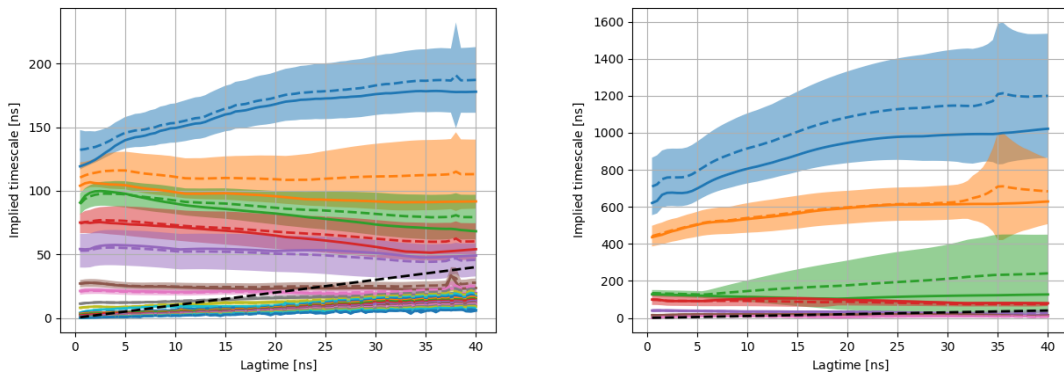


Figure S5: Implied time scales (ITS) for the interconversion processes of peptide **4** as described by CSMMs in water (left) and chloroform (right). The ITS of the whole data set is shown as solid line. The average (dashed line) and standard deviation (shaded area) were estimated with bootstrapping. Due to the very slow interconversion process in chloroform, two bootstrap samples had to be excluded to get converged results at high lag times.

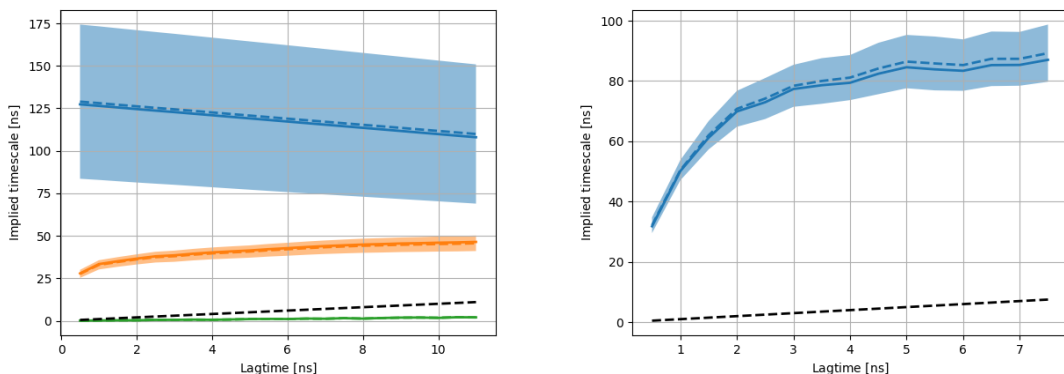


Figure S6: Implied time scales (ITS) for the interconversion processes of peptide **5** as described by CSMMs in water (left) and chloroform (right). The ITS of the whole data set is shown as solid line. The average (dashed line) and standard deviation (shaded area) were estimated with bootstrapping.

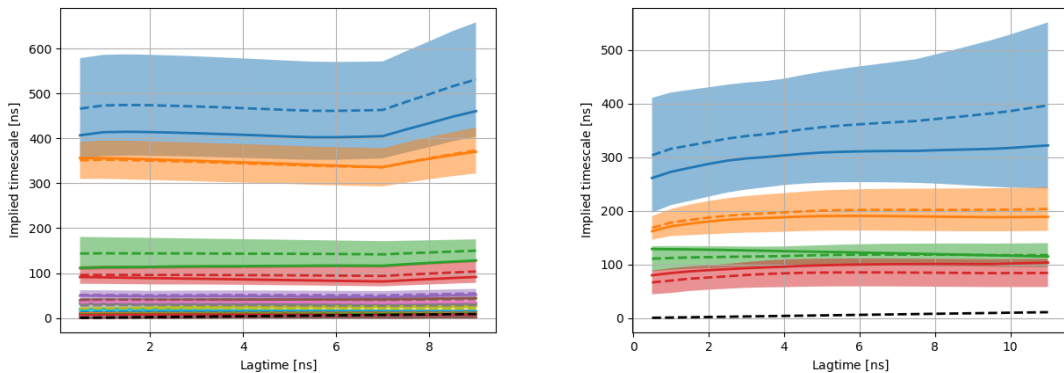


Figure S7: Implied time scales (ITS) for the interconversion processes of peptide **6** as described by CSMMs in water (left) and chloroform (right). The ITS of the whole data set is shown as solid line. The average (dashed line) and standard deviation (shaded area) were estimated with bootstrapping.

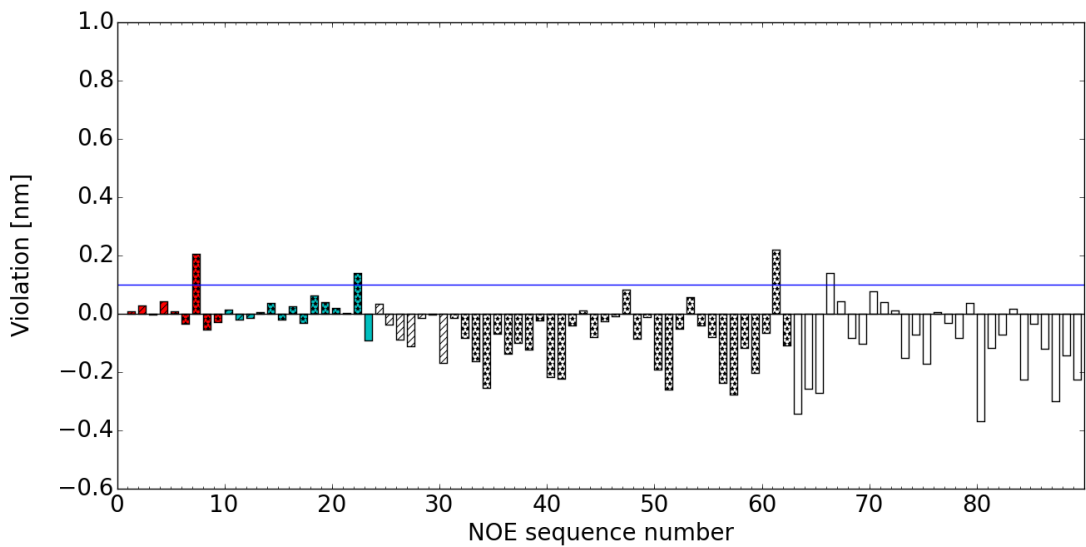


Figure S8: Violations of the experimental NOE upper distance bounds as a function of the NOE sequence number for the whole simulation of MKI in  $\text{CHCl}_3$ . The NOE distances are grouped into “intercycle” (red), “intermediate” (cyan), and NOE distances from neighboring or the same residues (white), and they are labeled on the basis of the nature of the protons: backbone–backbone (stripes), backbone–side chain (dots), and side chain–side chain (plain).

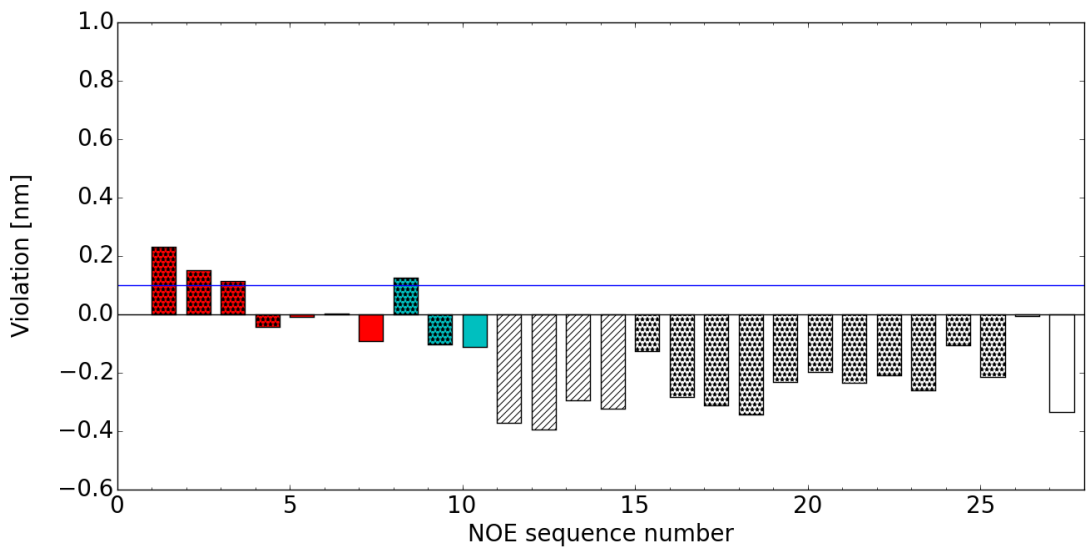


Figure S9: Violations of the experimental NOE upper distance bounds as a function of the NOE sequence number for the whole simulation of MII in  $\text{CHCl}_3$ . The NOE distances are grouped into “intercycle” (red), “intermediate” (cyan), and NOE distances from neighboring or the same residues (white), and they are labeled on the basis of the nature of the protons: backbone–backbone (stripes), backbone–side chain (dots), and side chain–side chain (plain).

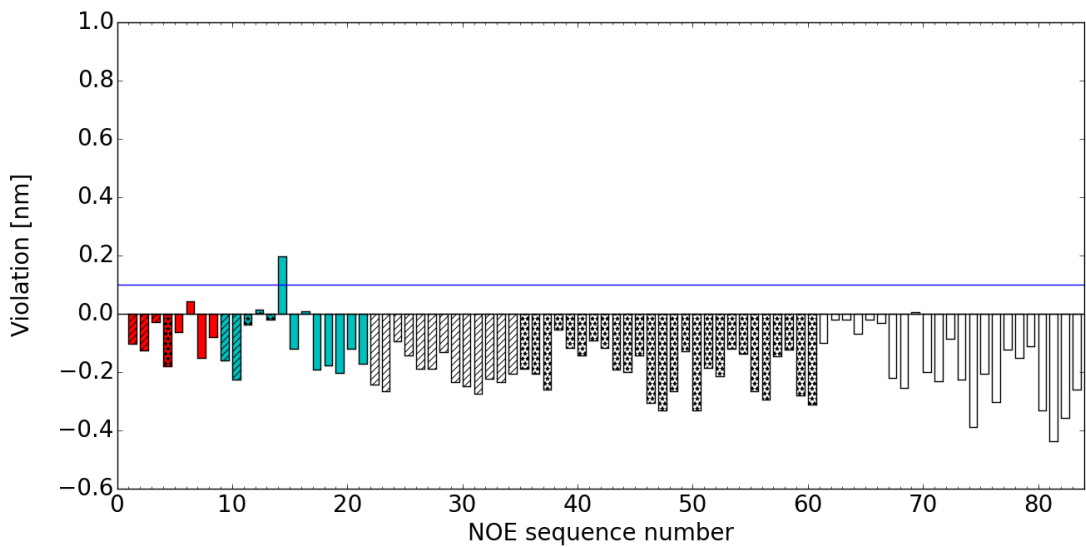


Figure S10: Violations of the experimental NOE upper distance bounds as a function of the NOE sequence number for the whole simulation of MHQ in  $\text{CHCl}_3$ . The NOE distances are grouped into “intercycle” (red), “intermediate” (cyan), and NOE distances from neighboring or the same residues (white), and they are labeled on the basis of the nature of the protons: backbone–backbone (stripes), backbone–side chain (dots), and side chain–side chain (plain).

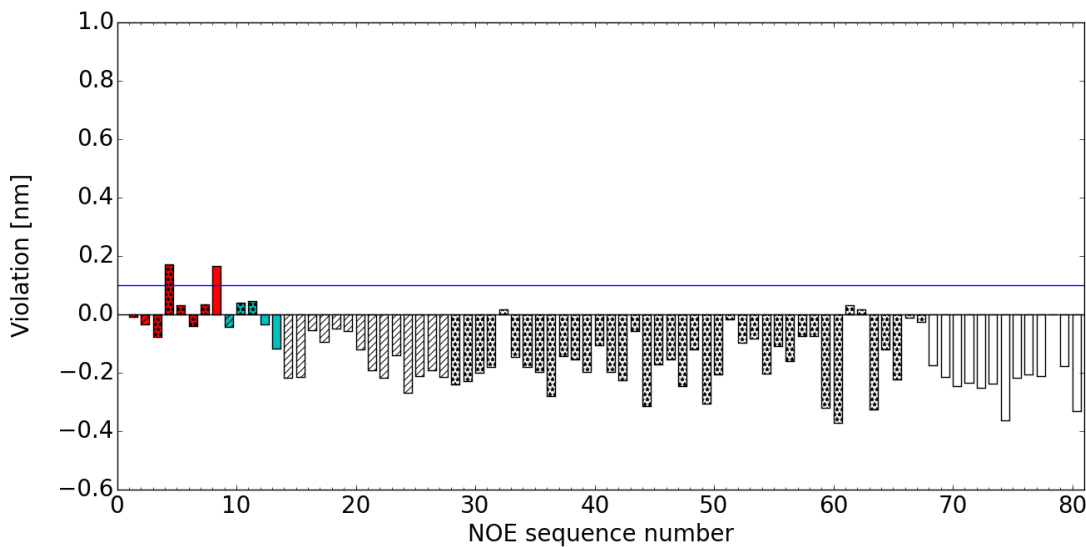


Figure S11: Violations of the experimental NOE upper distance bounds as a function of the NOE sequence number for the whole simulation of MDP in  $\text{CHCl}_3$ . The NOE distances are grouped into “intercycle” (red), “intermediate” (cyan), and NOE distances from neighboring or the same residues (white), and they are labeled on the basis of the nature of the protons: backbone–backbone (stripes), backbone–side chain (dots), and side chain–side chain (plain).

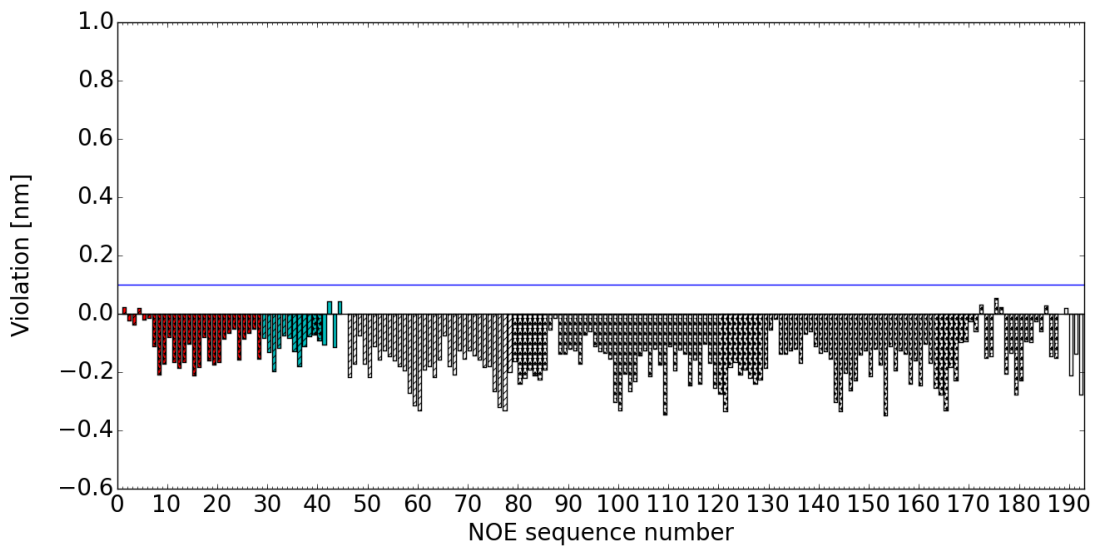


Figure S12: Violations of the experimental NOE upper distance bounds as a function of the NOE sequence number for the whole simulation of MDR in  $\text{CHCl}_3$ . The NOE distances are grouped into “intercycle” (red), “intermediate” (cyan), and NOE distances from neighboring or the same residues (white), and they are labeled on the basis of the nature of the protons: backbone–backbone (stripes), backbone–side chain (dots), and side chain–side chain (plain).

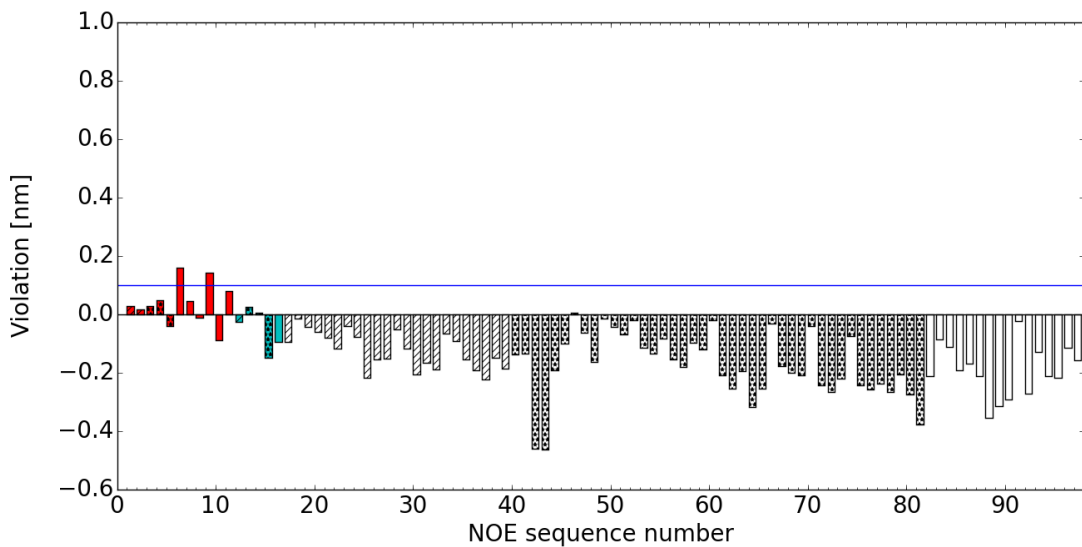


Figure S13: Violations of the experimental NOE upper distance bounds as a function of the NOE sequence number for the whole simulation of MJI in  $\text{CHCl}_3$ . The NOE distances are grouped into “intercycle” (red), “intermediate” (cyan), and NOE distances from neighboring or the same residues (white), and they are labeled on the basis of the nature of the protons: backbone–backbone (stripes), backbone–side chain (dots), and side chain–side chain (plain).

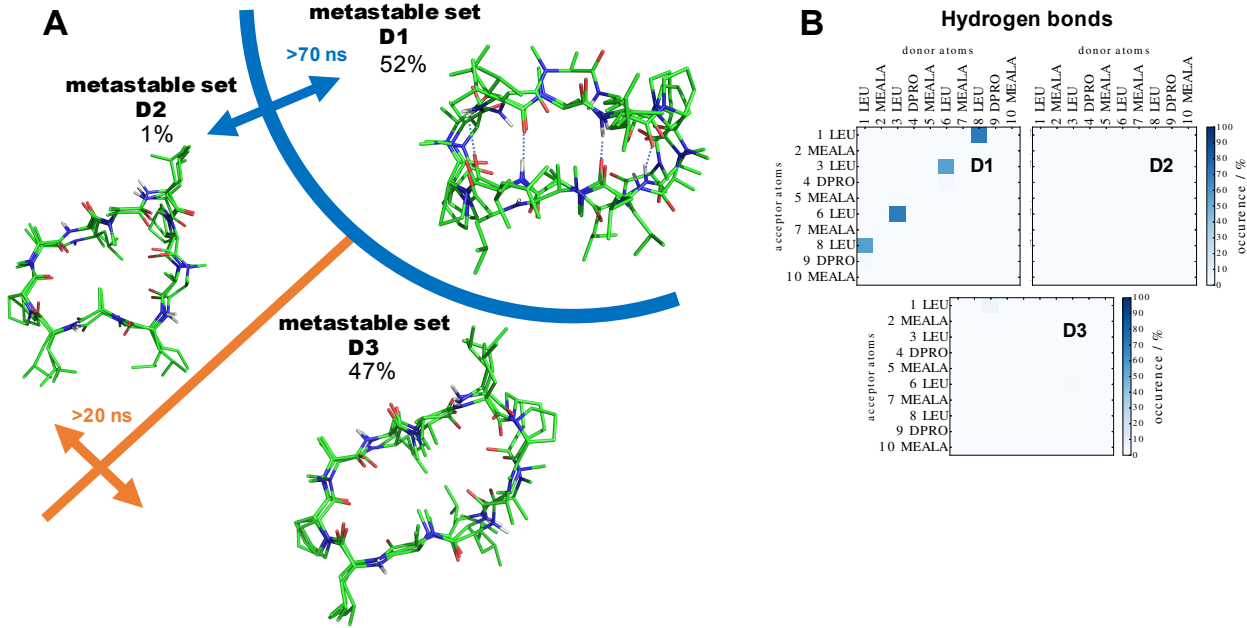


Figure S14: Metastable sets of MII in DMSO. (A) Schematic representation of the CSMM. The lines separating metastable sets correspond to interconversion processes occurring in the system. Three representative structures were randomly picked from each metastable set. Note that the population of a metastable state comprises that of the assigned core sets as well as the fuzzy assignment of the intermediate space to these core sets. (B) Patterns of backbone-backbone H-bonds observed.

## References

- (1) Vonkienlin, M.; Moonen, C. T. W.; Vandertoorn, A.; Vanzijl, P. C. M. Rapid Recording of Solvent-Suppressed 2D COSY Spectra with Inherent Quadrature Detection Using Pulsed Field Gradients. *J. Magn. Reson.* **1991**, *93*, 423–429.
- (2) Carpenter, T. A.; Colebrook, L. D.; Hall, L. D.; K.Pierens, G. Applications of Gradient-Selective COSY and DQCOSY to Brucine and Gibberellic-Acid. *Magn. Reson. Chem.* **1992**, *30*, 768–773.
- (3) Kay, L. E.; Keifer, P.; Saarinen, T. Pure Absorption Gradient Enhanced Heteronuclear Single Quantum Correlation Spectroscopy with Improved Sensitivity. *J. Am. Chem. Soc.* **1992**, *114*, 10663–10665.
- (4) Lindorff-Larsen, K.; Piana, S.; Palmo, K.; Maragakis, P.; Klepeis, J. L.; Dror, R. O.; Shaw, D. E. Improved Side-Chain Torsion Potentials for the Amber ff99SB Protein Force Field. *Proteins* **2010**, *78*, 1950–1958.
- (5) Kupce, E. Applications of adiabatic pulses in biomolecular nuclear magnetic resonance. *Method. Enzymol.* **2001**, *338*, 82–111.
- (6) Bax, A.; Summers, M. F. H-1 and C-13 Assignments from Sensitivity-Enhanced Detection of Heteronuclear Multiple-Bond Connectivity by 2D Multiple Quantum NMR. *J. Am. Chem. Soc.* **1986**, *108*, 2093–2094.

- (7) Meissner, A.; Sorensen, O. W. Economizing spectrometer time and broadband excitation in small-molecule heteronuclear NMR correlation spectroscopy. Broadband HMBC. *Magn. Reson. Chem.* **2000**, *38*, 981–984.
- (8) Bax, A.; Davis, D. G. Practical Aspects of Two-Dimensional Transverse NOE Spectroscopy. *J. Magn. Reson.* **1985**, *63*, 207–213.
- (9) Hwang, T. L.; Shaka, A. J. Cross Relaxation without TOCSY - Transverse Rotating-Frame Overhauser Effect Spectroscopy. *J. Am. Chem. Soc.* **1992**, *114*, 3157–3159.
- (10) Bax, A.; Davis, D. G. Mlev-17-Based Two-Dimensional Homonuclear Magnetization Transfer Spectroscopy. *J. Magn. Reson.* **1985**, *65*, 355–360.
- (11) Meissner, A.; Sorensen, O. W. Measurement of  $J(H,H)$  and long-range  $J(X,H)$  coupling constants in small molecules. Broadband XLOC and J-HMBC. *Magn. Reson. Chem.* **2001**, *39*, 49–52.
- (12) Meiboom, S.; Gill, D. Modified Spin-Echo Method for Measuring Nuclear Relaxation Times. *Rev. Sci. Instrum.* **1958**, *29*, 688–691.
- (13) Gottlieb, H. E.; Kotlyar, V.; Nudelman, A. NMR chemical shifts of common laboratory solvents as trace impurities. *J. Org. Chem.* **1997**, *62*, 7512–7515.
- (14) Herrmann, T.; Güntert, P.; Wüthrich, K. Protein NMR structure determination with automated NOE-identification in the NOESY spectra using the new software ATNOS. *J. Biomol. NMR* **2002**, *24*, 171–189.
- (15) Herrmann, T.; Güntert, P.; Wüthrich, K. Protein NMR structure determination with automated NOE assignment using the new software CANDID and the torsion angle dynamics algorithm DYANA. *J. Mol. Biol.* **2002**, *319*, 209–227.
- (16) Güntert, P. Automated NMR structure calculation with CYANA. *Methods Mol. Biol.* **2004**, *278*, 353–378.
- (17) Pearlman, D. A.; Case, D. A.; Caldwell, J. W.; Ross, W. S.; III, T. E. C.; DeBolt, S.; Ferguson, D.; Seibel, G.; Kollman, P. AMBER, a package of computer programs for applying molecular mechanics, normal mode analysis, molecular dynamics and free energy calculations to simulate the structural and energetic properties of molecules. *Comp. Phys. Commun.* **1995**, *91*, 1–41.
- (18) Bashford, D.; Case, D. A. Generalized born models of macromolecular solvation effects. *Annu. Rev. Phys. Chem.* **2000**, *51*, 129–152.
- (19) Darden, T.; York, D.; Pedersen, L. An  $N \cdot \log(N)$  Method for Ewald Sums in Large Systems. *J. Chem. Phys.* **1993**, *98*, 10089–10092.
- (20) Ryckaert, J.-P.; Ciccotti, G.; Berendsen, H. J. C. Numerical Integration of the Cartesian Equations of Motion of a System with Constraints: Molecular Dynamics of n-Alkanes. *J. Comput. Phys.* **1977**, *23*, 327–341.

- (21) Kansy, M.; Senner, F.; Gubernator, K. Physicochemical High Throughput Screening: Parallel Artificial Membrane Permeation Assay in the Description of Passive Absorption Processes. *J. Med. Chem.* **1998**, *41*, 1007–1010.